Enhanced Nonlinear Optical Coefficients of $MAPbI_3$ Thin Films by Bismuth Doping

C. Redondo-Obispo[1], I. Suárez[1,2], S.J. Quesada[1], T.S. Ripolles[1], J. P. Martínez-Pastor[2], A. L. Álvarez[1], A. de Andrés[3] and Carmen Coya*[1]

[1]Escuela Técnica Superior de Ingeniería de Telecomunicación, Universidad Rey Juan Carlos, C/Tulipán s/n, 28933 Madrid, Spain.

[2] UMDO, Instituto de Ciencia de los Materiales, Universidad de Valencia, 46071 Valencia, Spain

[3]Instituto de Ciencia de Materiales de Madrid, Consejo Superior de Investigaciones Científicas, C/ Sor Juana Inés de la Cruz 3, 28049 Madrid, Spain.

AUTHOR INFORMATION

Email: carmen.coya@urjc.es

ABSTRACT. The poor photo stability under ambient conditions of hybrid halide perovskites has hindered their recently explored promising nonlinear optical properties. Here, we show how Bi^{3+} can partially substitute Pb^{2+} homogenously in the commonly studied $MAPbI_3$ improving both environmental stability and photo-stability under high laser irradiation. Bi content around 2 at. % produces thin films where the nonlinear refractive (n_2) and absorptive coefficients (β), that modify the refractive index (Δn) of the material with light fluency (I), increase up to factors 4 and 3.5 respectively compared to undoped $MAPbI_3$. Higher doping inhibits the nonlinear parameters, however, the samples show higher fluency damage thresholds. Thus, these results show a roadmap on how $MAPbI_3$ can be engineered for practical cost-effective nonlinear applications, by means of Bi doping including optical limiting devices and multiple-harmonic generation into optoelectronics devices.

Graphical TOC

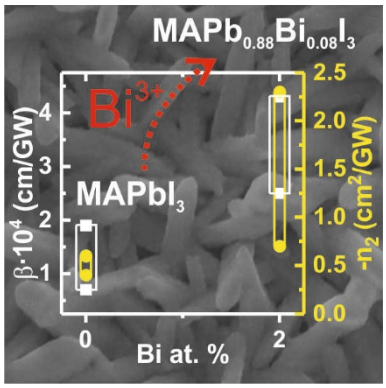

KEY WORDS: lead halide hybrid perovskites, bismuth doping, non-linear optical properties, XANES, NMR, Z-Scan.

Beyond the well-known excellent properties of hybrid metal halide perovskite (MHP) materials in cost effective photovoltaic devices[1] and optical sources,[2] also they have recently been investigated as a potential nonlinear media.[3, 4] With higher third order nonlinear coefficients than silicon,[5] these MHPs materials result interesting candidates as optical modulators,[6] harmonic generators[7] or saturable absorbers,[8] among other devices. The high absorption coefficient and high emission efficiency together with their technological feasibilities, suggest the possibility to combine these functionalities with nonlinear optical properties for the development of more sophisticated optoelectronic/photonic devices.[9] However, the chemical instability and fast degradation under ambient conditions[10, 11] prevent their practical applications. This limitation is even more restrictive in nonlinear devices, where the high irradiation fluencies required to observe the nonlinear effects result in faster degradation rate.

Within this context, the doping strategy, in particular the partial replacement of the lead cation in $MAPbI_3$, has been extensively studied to improve stability among other properties.[12-14] In particular, the strategy of heterovalent doping with bismuth is an interesting option because it possesses ionic radii similar to that of $Pb^{2+}$and isoelectronic configuration.[14-16] By means of first principle studies, Mosconi et al.[17] showed that bismuth acts as deep electron traps, and that the absorption onset red-shift observed upon Bi-doping of $MAPbI_3$ is mainly related to Bi defect states, while the perovskite band gap is essentially unaltered. Also, a recent work by Yavari et al.[18] established that Bi introduces both, shallow and deep electronics states in the bandgap which are responsible for the increased Shockley-Read-Hall recombination and therefore reduce the open-circuit voltage and luminescence yields. Besides, almost in parallel, we have shown that the incorporation up to 5 at. % of Bi^{3+} in the $MAPbI_3$ perovskite lattice leads to an enormous increase in photo stability without distorting the crystal structure,[19]

enabling to use around 1000 times higher laser irradiation intensity and for 6 times longer, without degrading the sample, which may be very appropriate for the perovskite-based optoelectronics devices mentioned above.

In this work, we show how Bi doping alters the third-order nonlinear properties of $MAPbI_3$. First, we thoroughly confirm the homogenous distribution of Bi^{3+} in the perovskite lattice by means of X-Ray diffraction (XRD), nuclear magnetic resonance (NMR) and X-ray absorption near edge structure (XANES) spectroscopies. We present, for the first time the XANES Bi L-III edge spectra not reported to date in hybrid perovskite derivatives. The study of the time evolution of XRD and optical absorption followed in Bi-doped $MAPbI_3$ thin films demonstrates a stability enhancement with doping under ambient conditions. Then, the nonlinear optical refraction and absorption are characterized, revealing an interesting dependence with the composition. Samples with Bi content of 2 at. %, present an enhancement of the nonlinear optical parameters, compared to those recorded from the standard $MAPbI_3$. Further doping results in the inhibition of the nonlinear parameters, although these samples show higher damage thresholds that could be useful to implement solar concentrators. Therefore, these results show a roadmap of how $MAPbI_3$ can be engineered for practical nonlinear applications by means of the Bi content.

Structural and morphological study. Bismuth-doped $MAPbI_3$ thin films were synthesised using the method described elsewhere.[19] Briefly, MAI, PbI_2 and BiI_3 precursor were mixed at 60 ºC in anhydrous DMF (40 wt. %) with stoichiometry $MA(Pb_{1-1.5x}Bi_x\square_{0.5x})I_3$, where □ stands for cation vacancy. Thin films have been synthesised with nominal at. % Bi of 0 (the reference $MAPbI_3$), 8, 13 and 18. Solutions were spin coated at 1500 rpm for 45 seconds and baked at 100 ºC for one hour on glass or borosilicate substrates for electrical and optical and non-linear optical properties

studies, respectively. Final Bi content in the perovskite crystal lattice was found to be substantially lower than the nominal precursor amount in the feed solution.[13, 19] Deep XRD analysis of thin films allowed us to estimate the actual amount of Bi^{3+} inside the perovskite lattice in a recent work[19] (nomenclature and compositions are summarized in Table S1 of Supplementary Information (SI)), resulting in 0, 2, 4 and 5 at. % Bi corresponding with samples 0, 8, 13 and 18 nominal at. % Bi respectively. From now on, samples are named as 0%Bi, 2%Bi, 4%Bi and 5%Bi.

XRD patterns of the 0%Bi-5%Bi thin films can be seen in Figure S1. The structure corresponds to the tetragonal *I4cm* space group, considering a polar tetragonal structural model, where the C−N bonds of the methylammonium cations are fixed parallel to the c-axis.[20] Note that in the diffractograms of samples 4%Bi-5%Bi reflections corresponding with hexagonal spurious $MA_3Bi_2I_9$ (blue vertical lines in Figure S1) are detected. An important consequence of bismuth doping was the absence of spurious PbI_2 in the XRD patterns.

We can define an effective or pondered ionic radii for the cation in B position (See SI for details), r_B, that allows us to estimate the Goldschmidt's tolerance factor *t* (Table S1) that approaches t=0.9 with bismuth increasing content, leading in principle to a more stable material. [21, 22]

Bi^{3+} addition induces the formation of rod-shaped structures whose aspect ratio (length/width) decreases with Bi content (SEM images, Figure S2a-c) related to the reported decrease of the preferential orientation fraction[19] that relaxes the growth habits allowing more rounded shapes. However, despite of this observed different grain sizes, crystallite size remains at about 90 nm in all samples.

Figure 1 shows the evolution with time of the integrated area, normalized to initial value, of the $MAPbI_3$ [110] reflection at 14.2 deg for 0%Bi-4%Bi thin films under ambient conditions (293 K, <30%RH) up to 1500 h. Between measurements, samples are maintained in dark at clean room ambient conditions, i.e. 298K and an average of <30%RH. For the undoped sample the perovskite phase degrades faster than for those with bismuth. Results for sample 5%Bi are not shown as this composition presents a significant fraction of the hexagonal spurious $MA_3Bi_2I_9$ phase (Figure S1).

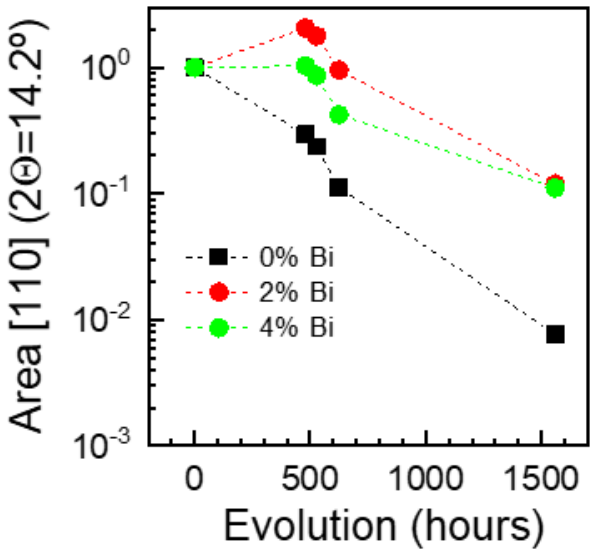

Figure 1. Evolution with time of the normalized integrated area of $MAPbI_3$ [110] reflection at 14.2 deg for 0%Bi-4%Bi thin films under ambient conditions (293 K) for up to 1500 h.

X-ray absorption near edge spectroscopy (XANES) measurements were performed at the European Synchrotron Radiation Facility (ESRF) for the 0%Bi-5%Bi thin films in order to confirm the predominant valence of bismuth (see the SI for details). XANES reports on the coordination environment of the absorbing atom, influenced by bonds nature, distances and coordination geometry. Figure 2a-b presents the Pb L-III edge spectra of undoped and Bi doped (0%Bi-5%Bi) samples which are essentially identical and exhibit weak peaks at 13056, 13063 and 13088 eV (See Figure 2a for normalized XANES spectra). Similar spectra have been reported by Sharenko et al.[23] for $MAPbI_3$

precursor solution and the three peaks are associated to iodoplumbate PbI_6^{4-}-like complexes. The presence of Pb in PbI_2 environment can be ruled out since, in this case, near-edge Pb-LIII consists of two large peaks at 13050 and 13082 eV.[23] Therefore, it seems that doping up to 5 at. % Bi does not induce appreciable modifications into the Pb coordination sphere in the perovskite lattice.

The XANES Bi L-III edge spectra for 2%Bi-5%Bi samples, not reported to date in lead halide perovskites derivatives, is shown in Figure 2c, consist in two peaks at around 13443 and 13478 eV, with slightly increasing intensity with Bi content. The similarity of the measured spectra for 2%Bi-5%Bi samples indicates that Bi environment is similar in all samples. These edge spectra are compared to a measured Bi_2O_3 reference (Bi^{3+} standard) peaking at 13440 and 13490 eV. The higher energy of this second peak in Bi_2O_3 than in 2%Bi-5%Bi samples is compatible with the fact that Bi-O bond typical distances (~2.2-2.3 Å) in Bi_2O_3 polymorphs[24] are much sorter that those reported for Bi-I bond length in BiI_3 compound (3-3.12 Å[25] or 3.09 Å in $MA_3Bi_2I_9$). Similar energy sift is observed in standard bismuth oxides samples with different Bi-O lengths (e.g. Bi_2O_3 (Bi^{3+}), $NaBiO_3$ (Bi^{5+})).[24, 26] We can assume then a regular replacement of Pb (II) by Bi (III).

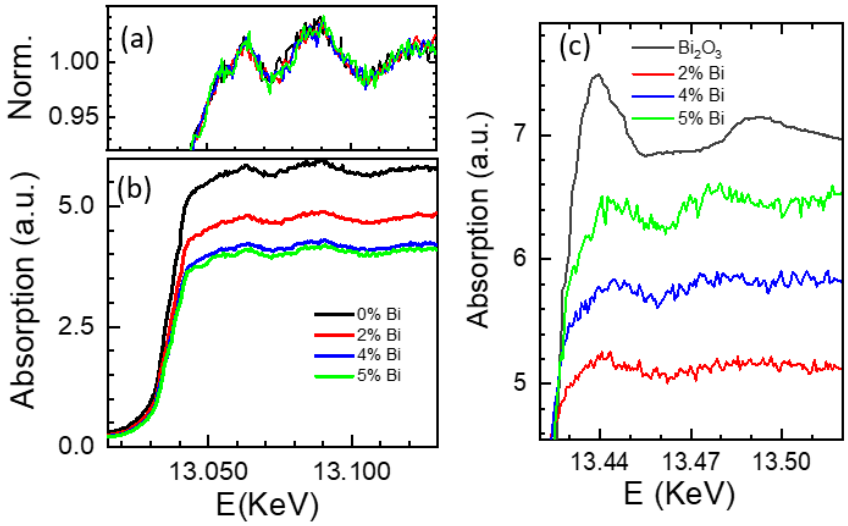

Figure 2. Pb L-III edge X-ray absorption near edge structure (XANES) spectra of the measured samples. (a) normalized Pb L-III edge of 0%Bi-5%Bi samples, (b) Pb L-III edge of 0%Bi-5%Bi samples and (c) Bi-LIII edge of 2%Bi-5%Bi samples and Bi_2O_3 reference.

To further investigate the homogenous presence of Bi, static spin echo solid-state NMR spectra were recorded for the undoped (0%Bi) and doped $MAPbI_3$ (5%Bi) crystals grown for this purpose (see SI). ^{1}H NMR spectra of samples 0%Bi and 5%Bi are shown in Figure 3a. We can observe that doping with Bi does not produce a significant broadening of the peaks but a displacement downfield, compatible with variations in the chemical environment of MA cations, while maintaining the crystalline order.[27-29] We also present the unreported ^{209}Bi NMR solid state spectra for Bi-doped $MAPbI_3$ in Figure 3b. Here, the large nuclear quadrupole moment and electric field gradients at the Bi site lead to peak multiplicity and line shapes, even in the most spherically symmetric environments. The quadrupolar interaction is important in the sense that electric field gradients arising from surrounding atoms and bonds are sensitive to even minor structural changes, providing information on the spherical and axial symmetry.[30] The smaller quadrupolar interaction in sample 5%Bi reflects the higher spherical symmetry of the electronic charge distribution about the Bi atom compared to those in single-bismuth-site $Bi(NO_3)_3$ reference.

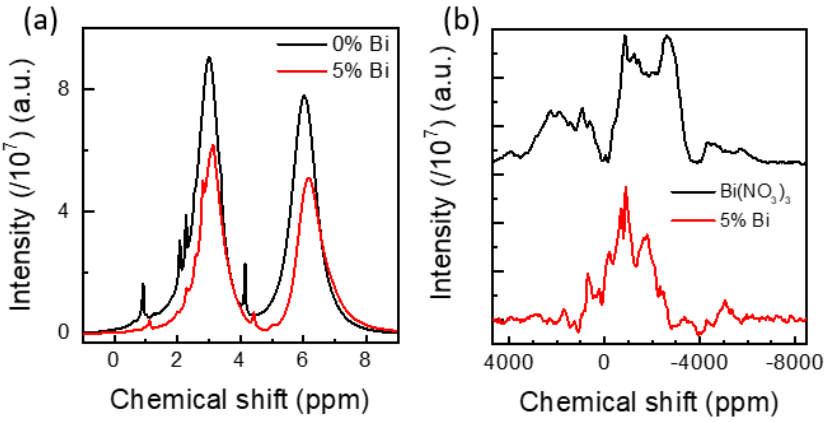

Figure 3. Static spin echo solid-state NMR spectrum of samples 0%Bi and 5%Bi crystals showing (a) ^{1}H spectra and (b) ^{209}Bi spectra of the Bi-doped $MAPbI_3$ and the used reference $Bi(NO)_3$.

Optical absorption. Optical absorption spectra of the 0%Bi-5%Bi thin films deposited on glass were measured in the 1.5-4 eV range (Figure 4a). These absorbance spectra are in agreement with those reported results for $MAPbI_3$, which showed an absorption coefficient around 10^5 cm^{-1}.[31] Bismuth addition increases the absorption coefficient value, α above the band gap. Bi^{3+} does not induce changes in the band gap energy, E_g, compared to standard $MAPbI_3$ as it is deduced from optical absorption spectra second derivatives (Figure S3). The first electronic transition, E_g, is at 1.6 eV ± 0.05 eV for all films (assuming the full width at half-maximum of the second derivative as the error) and it corresponds with reported values for $MAPbI_3$.[32] The extent of the absorption tail below the band gap (inset of Figure 4a) is intimately associated with the degree of energetic disorder within the material, which stems from thermal fluctuation of the ions involved or from defects in the perovskite structure.[33] Below E_g, the absorption coefficient follows an exponential trend, $\alpha \sim \alpha_0 \exp(h\nu/E_U)$, towards lower photon energies. The slope of this exponential region is the so-called Urbach energy, E_U.[33] Here, bismuth induces large change in this parameter compared with undoped-$MAPbI_3$

(see inset of Figure 4a and Figure 4b). This is consistent with the fact that Bi induces defect states and a significant increase in the sub-band-gap density of states, which are associated with the extent of the absorption tail below the band gap.[17, 19]

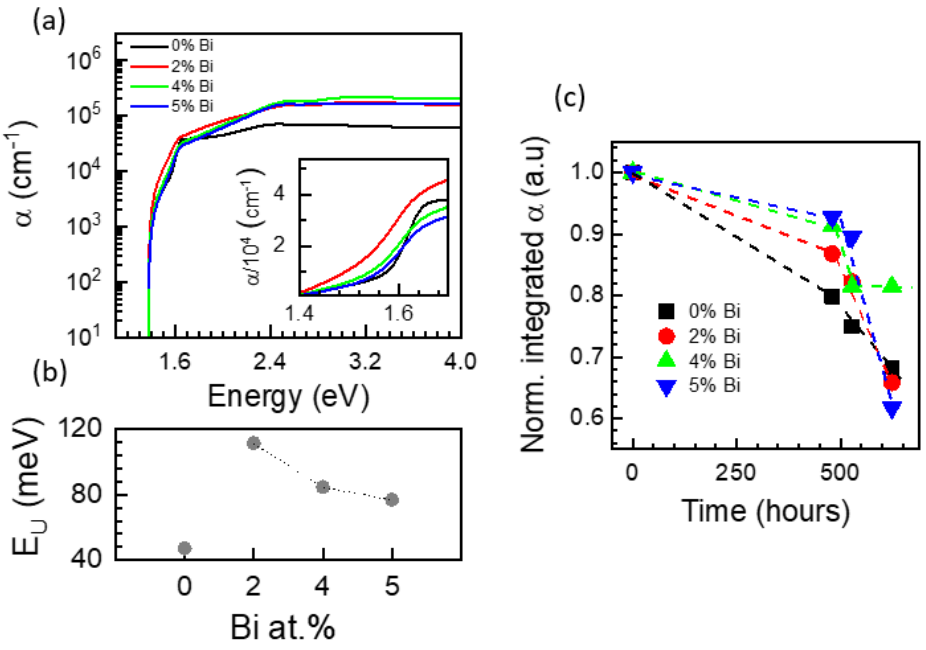

Figure 4. (a) Absorption coefficient spectra of 0%Bi-5%Bi thin films. The inset shows the absorption tail below the band gap. (b) Urbach energies versus Bi content and (c) Evolution with time of the integrated absorption coefficient (in the 1.4 to 4 eV range).

The evaluation of the changes in absorption coefficient, as thin films degrade in ambient conditions, confirms the stability improvement by increasing the Bi content as previously deduced by from XRD results. The integrated area of α in the 1.3-4 eV range has been calculated and represented in Figure 4c. Clearly, the smaller variation of the absorption coefficient in doped films indicates that Bi favours the stability under ambient conditions at RT. For the first 500 hours, α drops 20 % of its original value for the undoped sample, while this variation is much smaller for doped ones (samples 2%Bi-5%Bi). The evolution of second derivatives of the optical absorption is shown in

Figure S3. At 1500 h, all samples gradually evolve to PbI_2 since only a transition is present at 2.4-2.5 eV corresponding to the band gap transition of PbI_2.[34]

Nonlinear optical properties. The stability of the films under high laser excitation fluencies also demonstrates an improvement with Bi doping. Figure 5a shows the normalized transmittance, T, of the ns-pulsed laser beam at 1064 nm as a function of the excitation fluency (I) for all samples. For excitation fluencies above 0.15-0.2 GW/cm^2, T experiences a strong decrease with I for samples 0%Bi and 2%Bi that can be ascribed to the degradation of the film with the laser irradiation power.[35, 36] In fact, we observed a similar behaviour for other $MAPbI_3$ films exposed to similar excitation fluencies.[5] However, samples 4%Bi and 5%Bi preserve a flat response up to 0.3-0.4 GW/cm^2, indicating that the increase of the Bi content beyond 2 at. % leads to higher resistance of the film to the laser damage, which can be correlated with the higher stability of the perovskite in this case. A more detailed look at the 0-0.2 GW/cm^2 region (Figure 5b) reveals that for low excitations (I<0.1 GW/cm^2), T shows the characteristic flat response of any material under linear regime but for intermediate excitations (0.1<I<0.15 GW/cm^2), T can show a decrease with the excitation fluency due to the nonlinear absorption in 0%Bi and 2%Bi samples, as we have recently reported for MAPI films.[5] The efficiency of this mechanism depends on the Bi composition and it will be explained below.

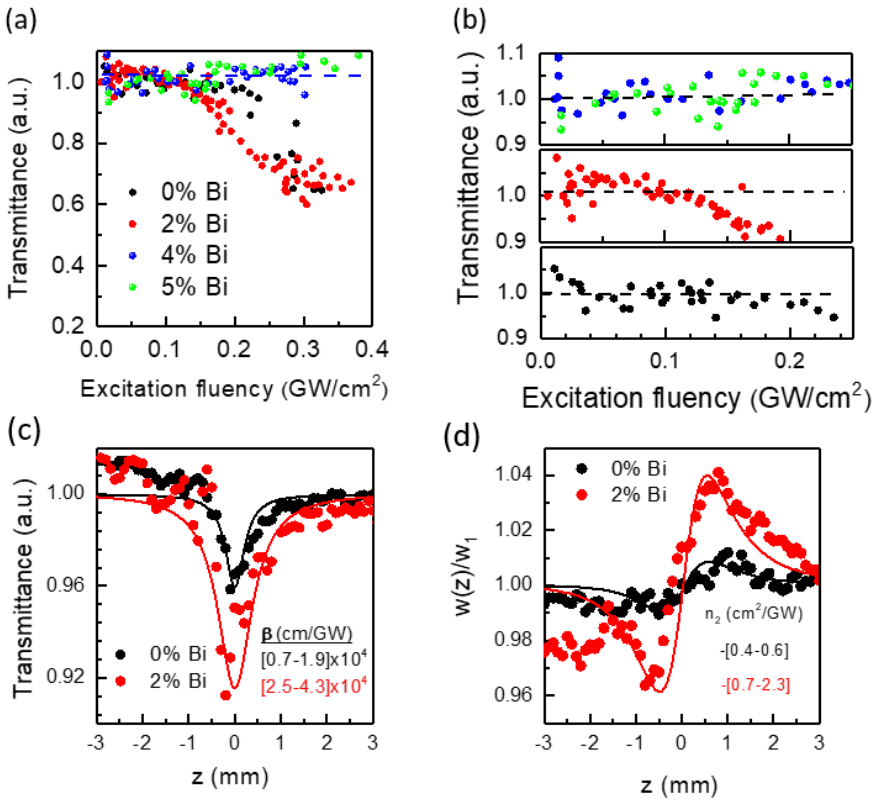

Figure 5. (a) Transmittance at 1064 nm through the 0%Bi-5%Bi samples as a function of the excitation fluency. (b) Zoom of the 0-0.2 GW/cm^2 region for the sake of clarity. Dashed lines are guides for the eyes. (c)-(d) Representative Z-scan measurements after the FFT treatment according the method described in ref [5]. Black and red symbols correspond to the experimental data obtained from 0%Bi and 2%Bi thin films, respectively. Solid lines correspond to the fitting. a) Open aperture Z-scan where the nonlinear absorption (β) is obtained. b) Image Z-scan, the evolution of the normalized waist ($W(z)/W_1$, W_1 refers to waist for $|z| >> z_0$) of the beam where the nonlinear refraction (n_2) is obtained.

The transmitted light under high excitation fluencies was recorded as a function of the sample position (Z) in such a way that the intensity of the excitation beam is gradually increased and decreased by a lens (see experimental section in SI for details). Then, non-linear absorption coefficient can be obtained by integrating the whole intensity

(open aperture Z-scan), while the non-linear refraction can be analyzed by integrating the transmittance through a finite aperture in the center of the spot (closed aperture Z-scan).[37] For the excitation beam here used (1064 nm focused on 11-13 μm) the Rayleigh length (z_0) becomes 350 μm, longer than the thickness of the sample (500 nm), hence fulfilling the thin sample approximation condition (see SI to see the details of the Z-scan measurement).[37] In this way, z was ranged between $-10 \cdot z_0$ to $10 \cdot z_0$ in order to analyse the transmitted light for low ($z \ll z_0$) and high ($z \sim z_0$) excitation fluencies. In these conditions, Z-scan set-up provides the estimation of both the refractive (n_2) and absorptive coefficients (β), that modify the refractive index (Δn) of the material with the intensity of light (I) by:

$$\Delta n = n_2 \cdot I - i \cdot \frac{\lambda}{4 \cdot \pi} \cdot \beta_2 \cdot I \quad (1)$$

where λ is the operation wavelength. According to Figure 5a, in order to prevent the degradation of the samples in the characterization of the nonlinear parameters by Z-scan measurements, the excitation fluency was limited to a value of 0.14 GW/cm^2, i.e. below the damage threshold for samples 0%Bi and 2%Bi.

The open aperture Z-scan analysis for sample 0%Bi, corresponding to standard $MAPbI_3$ (black symbols in Figure 5c) reveals a dip in $z=0$, which is characteristics of a material with non-negligible nonlinear absorption (β). A FFT treatment of the Z-scan data was applied in order to minimize light scattering (or other non-desirable effects) inherent to the characterization of polycrystalline thin films, as explained elsewhere.[5] Indeed, experimental data can be nicely fitted (black line) with β ranged between 0.7×10^4 and 0.9×10^4 cm/GW, in agreement with results recently published,[5] and previous works in the literature.[4] Nevertheless, a similar characterization on sample 2%Bi clearly indicates

a significant enhancement (up to a factor 4) of the nonlinear absorption by a deeper dip (red symbols in Figure 5c), that can be nicely fitted with $\beta = 2.5\times10^4$ -4.3×10^4 cm/GW.

In the same way, closed aperture Z-scan spectra (Figure 5d) in samples 0%Bi-2%Bi exhibit the characteristic peak-valley curve typical of a material with significant nonlinear refraction (n_2). Then, the sample acts a z-dependent lens, where the waist of the beam (W(z)) is focused and defocused from the initial width (W_1). In this way, the evolution of the normalized beam width (W/W_1) shows the complementary valley-peak curve, chosen here to increase the accuracy in the determination of the nonlinear parameters by a FFT treatment.[5] Here, the absolute value of n_2 depends on the peak valley separation, while the sign changes the peak-valley ($n_2<0$) or valley-peak ($n_2>0$) shape of the curve. Clearly sample 2%Bi present a higher nonlinear coefficient (a factor 3.5) than the standard perovskite, sample 0%Bi, as observed in the Figure 5d by a longer peak-valley distance. Indeed, the fitting in the different samples/measurements indicates that n_2=-[0.4-0.6] cm^2/GW and n_2=-[0.7-2.7] cm^2/GW for 0%Bi and 2%Bi, respectively. The negative sign in n_2 follows the trend determined by the n_2-$h\nu/E_g$ relationship predicted in a band to band model,[38] while the coefficients obtained for the $MAPbI_3$ reference, 0%Bi sample, agree with those reported in the literature under similar excitation conditions.[5]

For samples with higher Bi content (4%Bi and 5%Bi), however, nonlinear parameters could not be extracted. Indeed, the same experiment under an excitation fluency of 0.35 GW/cm^2 did not show nonlinear response either. We speculate that the loss of crystallinity with the addition of Bi[19] could be detrimental to the generation of second-order effects. Therefore, although Bi content improves sample stability in ambient conditions, for non-linear applications the incorporation of Bi is limited to 2 at. %. At this composition, 2 at. % Bi, $CH_3NH_3Pb_{0.88}Bi_{0.08}I_3$, both the nonlinear coefficients and

stability are improved. In this way, we suggest that these Bi-doped lead halide polycrystalline films are potential candidates to boost of a broad range of nonlinear applications such as optical limiting devices for high intense pulsed beams, where the material can absorb light without damage, or multiple-harmonic generation, where the excellent nonlinear refraction can improve the efficiency under high excitation fluencies.

Finally, it is interesting to compare the nonlinear properties measured with Bi doped MAPI with other emerging nonlinear materials, such us metal-organic frameworks (MOF),[39] Antimonene,[40] titanium disulphide (TiS_2)[41] or Mxene ($Ti_3C_2T_x$).[42] First of all, nonlinear absorption reported from these materials at excitation wavelengths close to 1064 nm under 100 fs excitation pulses ranges between $-3.86\cdot10^{-3}$ cm/GW [42] (MXene) and $-3.7\cdot10^{-2}$ cm/GW (MOF),[39] while β presented here for Bi doped MAPI is found between 2.5 and $4.3\cdot10^{4}$ cm/GW under 1 ns pulse width at 1064 nm. Secondly, MAPI shows a positive β¸indicative of two photon absorption process, which is characteristics for this family of semiconductors,[4] while TOF and MXene presents a negative β, useful for saturable absorption. In addition, the absolute value of β obtained here is always higher, even if the scalability of the nonlinear parameters with the pulse width (1 ns/100 fs = 10^4) would be taken into account.[43] Indeed, among these emerging materials, only TiS_2 exhibits a giant value of β ($-4.3\cdot10^{4}$ cm/GW), but obtained under much shorter excitation laser wavelength (400 nm). Concerning the nonlinear refractive index, n_2, reported values range between $-1.2\cdot10^{-6}$ cm^2/GW in MOFs[39] and $-3.47\cdot10^{-3}$ cm^2/GW for MXene,[41] both measured with lasers at 1064 nm and 100 fs pulses. Thus, they also show negative n_2 sign characteristic for MAPI,[4] but smaller absolute values (taking into account, again, the scalability with the pulse width).

In summary, a thoroughly structural characterization by means of XRD, XANES and NMR of Bi-doped $MAPbI_3$ layers supports that Bi^{3+} dopant is homogeneously distributed replacing Pb^{2+} up to 4 at. % into the $MAPbI_3$ lattice. These doped samples present more environmental stability as confirmed from X-ray diffraction patterns and optical absorbance evolution with time. The photo-stability of the films under high excitation fluencies also improves with Bi doping. Bi content around 2 at. % produces an optimum material where both the nonlinear optical coefficients and stability are improved. These findings pave the way for future use of these Bi-doped lead halide perovskite films as potential candidates to develop of a broad range of nonlinear optical applications including optical limiting devices and multiple-harmonic generation into optoelectronics devices.

Associated content

See supplementary material (Supporting Information) for experimental methods details, SEM images, XRD patterns and evolution of second derivative of absorption with time.

Acknowledgements

We acknowledge: financial support by the Spanish Ministerio de Economía y Competitividad (MINECO) under Projects MAT2015-65356-C3-2-R, TEC2017-86102-C2-1-R, ENE2017-90565-REDT National Excellence Network and University of Valencia via Project UV-INV-AE16-514545; Associated Lab LABCADIO belonging to CM net labs ref. 351. We also acknowledge the MINECO for financial support and provision of synchrotron radiation facilities at ESRF, and thank Eduardo Salas for his assistance in using Spanish beamline BM25A SpLine at The European Synchrotron (ESRF) and C. Force and S. Carralero for their technical assistance with NMR measurements. T. S. Ripolles. S.J. Quesada and C-D. Redondo acknowledge the

funding from Comunidad de Madrid and European Social Fund (ESF) under the Talento fellowship 2017-T2/IND-5586, postdoctoral PEJD-2017-POST/IND-3579 and under predoctoral PEJD-2018-PRE/IND-8839 Youth Employment Initiative (YEI), respectively.

References.

(1) Jena, A. K.; Kulkarni, A.; Miyasaka, T. Halide Perovskite Photovoltaics: Background, Status, and Future Prospects. *Chem. Rev.* **2019,** *119* (5), 3036-3103.
(2) Sutherland, B. R.; Sargent, E. H. Perovskite photonic sources. *Nat. Photon.* **2016,** *10*, 295.
(3) Xu, J.; Li, X.; Xiong, J.; Yuan, C.; Semin, S.; Rasing, T.; Bu, X. H. Halide Perovskites for Nonlinear Optics. *Adv. Mater.* **2019,** *32* (3), e1806736.
(4) Ferrando, A.; Martínez Pastor, J. P.; Suárez, I. Toward Metal Halide Perovskite Nonlinear Photonics. *J. Phys. Chem. Lett.* **2018,** *9* (18), 5612-5623.
(5) Suárez, I.; Vallés-Pelarda, M.; Gualdrón-Reyes, A. F.; Mora-Seró, I.; Ferrando, A.; Michinel, H.; Salgueiro, J. R.; Pastor, J. P. M. Outstanding nonlinear optical properties of methylammonium- and Cs-PbX_3 (X = Br, I, and Br–I) perovskites: Polycrystalline thin films and nanoparticles. *APL Mater.* **2019,** *7* (4), 041106.
(6) Grinblat, G.; Abdelwahab, I.; Nielsen, M. P.; Dichtl, P.; Leng, K.; Oulton, R. F.; Loh, K. P.; Maier, S. A. Ultrafast All-Optical Modulation in 2D Hybrid Perovskites. *ACS Nano* **2019,** *13* (8), 9504-9510.
(7) Abdelwahab, I.; Grinblat, G.; Leng, K.; Li, Y.; Chi, X.; Rusydi, A.; Maier, S. A.; Loh, K. P. Highly Enhanced Third-Harmonic Generation in 2D Perovskites at Excitonic Resonances. *ACS Nano* **2018,** *12* (1), 644-650.
(8) Zhang, R.; Fan, J.; Zhang, X.; Yu, H.; Zhang, H.; Mai, Y.; Xu, T.; Wang, J.; Snaith, H. J. Nonlinear Optical Response of Organic–Inorganic Halide Perovskites. *ACS Photonics* **2016,** *3* (3), 371-377.
(9) Zhang, Y.; Lim, C.-K.; Dai, Z.; Yu, G.; Haus, J. W.; Zhang, H.; Prasad, P. N. Photonics and optoelectronics using nano-structured hybrid perovskite media and their optical cavities. *Physics Reports* **2019,** *795*, 1-51.
(10) Ahmad, Z.; Najeeb, M. A.; Shakoor, R. A.; Alashraf, A.; Al-Muhtaseb, S. A.; Soliman, A.; Nazeeruddin, M. K. Instability in $CH_3NH_3PbI_3$ perovskite solar cells due to elemental migration and chemical composition changes. *Sci. Rep.* **2017,** *7* (1), 15406.
(11) Fu, Q.; Tang, X.; Huang, B.; Hu, T.; Tan, L.; Chen, L.; Chen, Y. Recent Progress on the Long-Term Stability of Perovskite Solar Cells. *Adv. Sci.* **2018,** *5* (5), 1700387.
(12) Frolova, L. A.; Anokhin, D. V.; Gerasimov, K. L.; Dremova, N. N.; Troshin, P. A. Exploring the Effects of the Pb^{2+} Substitution in $MAPbI_3$ on the Photovoltaic Performance of the Hybrid Perovskite Solar Cells. *J. Phys. Chem. Lett.* **2016,** *7* (21), 4353-4357.
(13) Abdelhady, A. L.; Saidaminov, M. I.; Murali, B.; Adinolfi, V.; Voznyy, O.; Katsiev, K.; Alarousu, E.; Comin, R.; Dursun, I.; Sinatra, L., et al. Heterovalent Dopant Incorporation for Bandgap and Type Engineering of Perovskite Crystals. *J. Phys. Chem. Lett.* **2016,** *7* (2), 295-301.
(14) Wang, R.; Zhang, X.; He, J.; Ma, C.; Xu, L.; Sheng, P.; Huang, F. Bi^{3+}-doped $CH_3NH_3PbI_3$: Red-shifting absorption edge and longer charge carrier lifetime. *J. Alloys Compd.* **2017,** *695*, 555-560.
(15) Zhou, Y.; Yong, Z.-J.; Zhang, K.-C.; Liu, B.-M.; Wang, Z.-W.; Hou, J.-S.; Fang, Y.-Z.; Zhou, Y.; Sun, H.-T.; Song, B. Ultrabroad Photoluminescence and Electroluminescence at New Wavelengths from Doped Organometal Halide Perovskites. *J. Phys. Chem. Lett.* **2016,** *7* (14), 2735-2741.

(16) Zhou, Y.; Yong, Z.-J.; Zhang, W.; Ma, J.-P.; Sadhanala, A.; Chen, Y.-M.; Liu, B.-M.; Zhou, Y.; Song, B.; Sun, H.-T. Ultra-broadband optical amplification at telecommunication wavelengths achieved by bismuth-activated lead iodide perovskites. *J. Mater. Chem. C* **2017,** *5* (10), 2591-2596.
(17) Mosconi, E.; Merabet, B.; Meggiolaro, D.; Zaoui, A.; De Angelis, F. First-Principles Modeling of Bismuth Doping in the $MAPbI_3$ Perovskite. *J. Phys. Chem. C* **2018,** *122* (25), 14107-14112.
(18) Yavari, M.; Ebadi, F.; Meloni, S.; Wang, Z. S.; Yang, T. C.-J.; Sun, S.; Schwartz, H.; Wang, Z.; Niesen, B.; Durantini, J., et al. How far does the defect tolerance of lead-halide perovskites range? The example of Bi impurities introducing efficient recombination centers. *J. Mater. Chem. A* **2019,** *7* (41), 23838-23853.
(19) Bartolomé, J.; Climent-Pascual, E.; Redondo-Obispo, C.; Zaldo, C.; Álvarez, Á. L.; de Andrés, A.; Coya, C. Huge Photostability Enhancement in Bismuth-Doped Methylammonium Lead Iodide Hybrid Perovskites by Light-Induced Transformation. *Chem. Mater.* **2019,** *31* (10), 3662-3671.
(20) Stoumpos, C. C.; Malliakas, C. D.; Kanatzidis, M. G. Semiconducting Tin and Lead Iodide Perovskites with Organic Cations: Phase Transitions, High Mobilities, and Near-Infrared Photoluminescent Properties. *Inorg. Chem.* **2013,** *52* (15), 9019-9038.
(21) Goldschmidt, V. M. Die Gesetze der Krystallochemie. *Naturwissenschaften* **1926,** *14*, 477-485.
(22) Synthesis, Structure, and Properties of Organic-Inorganic Perovskites and Related Materials. In *Progress in Inorganic Chemistry*, pp 1-121.
(23) Sharenko, A.; Mackeen, C.; Jewell, L.; Bridges, F.; Toney, M. F. Evolution of Iodoplumbate Complexes in Methylammonium Lead Iodide Perovskite Precursor Solutions. *Chem. Mater.* **2017,** *29* (3), 1315-1320.
(24) Jiang, N.; Spence, J. C. H. Can near-edge structure of the Bi L_3 edge determine the formal valence states of Bi? *J. Phys.: Condens. Matter* **2006,** *18* (34), 8029-8036.
(25) Phuyal, D.; Jain, S. M.; Philippe, B.; Johansson, M. B.; Pazoki, M.; Kullgren, J.; Kvashnina, K. O.; Klintenberg, M.; Johansson, E. M. J.; Butorin, S. M., et al. The electronic structure and band interface of cesium bismuth iodide on a titania heterostructure using hard X-ray spectroscopy. *J. Mater. Chem. A* **2018,** *6* (20), 9498-9505.
(26) Heald, S. M.; DiMarzio, D.; Croft, M.; Hegde, M. S.; Li, S.; Greenblatt, M. X-ray-absorption study of charge-density ordering in $(Ba_{1-x}K_x)BiO_3$. *Phys. Rev. B* **1989,** *40* (13), 8828-8833.
(27) McLeod, J. A.; Wu, Z.; Sun, B.; Liu, L. The influence of the I/Cl ratio on the performance of $CH_3NH_3PbI_{3-x}Cl_x$-based solar cells: why is $CH_3NH_3I : PbCl_2 = 3 : 1$ the "magic" ratio? *Nanoscale* **2016,** *8* (12), 6361-6368.
(28) Roiland, C.; Trippé-Allard, G.; Jemli, K.; Alonso, B.; Ameline, J.-C.; Gautier, R.; Bataille, T.; Le Pollès, L.; Deleporte, E.; Even, J., et al. Multinuclear NMR as a tool for studying local order and dynamics in $CH_3NH_3PbX_3$ (X = Cl, Br, I) hybrid perovskites. *Phys. Chem. Chem. Phys.* **2016,** *18* (39), 27133-27142.
(29) Senocrate, A.; Moudrakovski, I.; Maier, J. Short-range ion dynamics in methylammonium lead iodide by multinuclear solid state NMR and 127I NQR. *Phys. Chem. Chem. Phys.* **2018,** *20* (30), 20043-20055.
(30) Hamaed, H.; Laschuk, M. W.; Terskikh, V. V.; Schurko, R. W. Application of Solid-State ^{209}Bi NMR to the Structural Characterization of Bismuth-Containing Materials. *J. Am. Chem. Soc.* **2009,** *131* (23), 8271-8279.
(31) De Wolf, S.; Holovsky, J.; Moon, S.-J.; Löper, P.; Niesen, B.; Ledinsky, M.; Haug, F.-J.; Yum, J.-H.; Ballif, C. Organometallic Halide Perovskites: Sharp Optical Absorption Edge and Its Relation to Photovoltaic Performance. *J. Phys. Chem. Lett.* **2014,** *5* (6), 1035-1039.
(32) Shirayama, M.; Kadowaki, H.; Miyadera, T.; Sugita, T.; Tamakoshi, M.; Kato, M.; Fujiseki, T.; Murata, D.; Hara, S.; Murakami, T. N., et al. Optical Transitions in Hybrid Perovskite Solar Cells: Ellipsometry, Density Functional Theory, and Quantum Efficiency Analyses for $CH_3NH_3PbI_3$. *Phys. Rev. Appl.* **2016,** *5* (1), 014012.

(33) Urbach, F. The Long-Wavelength Edge of Photographic Sensitivity and of the Electronic Absorption of Solids. *Phys. Rev.* **1953,** *92* (5), 1324-1324.
(34) Agrawal, H.; Vedeshwar, A. G.; Saraswat, V. K. Growth and Characterization of PbI_2 Thin Films by Vacuum Thermal Evaporation. *JNanoR* **2013,** *24*, 1-6.
(35) Kanaujia, P. K.; Vijaya Prakash, G. Laser-induced microstructuring of two-dimensional layered inorganic–organic perovskites. *Phys. Chem. Chem. Phys.* **2016,** *18* (14), 9666-9672.
(36) Climent-Pascual, E.; Hames, B. C.; Moreno-Ramírez, J. S.; Álvarez, A. L.; Juarez-Perez, E. J.; Mas-Marza, E.; Mora-Seró, I.; de Andrés, A.; Coya, C. Influence of the substrate on the bulk properties of hybrid lead halide perovskite films. *J. Mater. Chem. A* **2016,** *4* (46), 18153-18163.
(37) Sheik-Bahae, M.; Said, A. A.; Wei, T.; Hagan, D. J.; Stryland, E. W. V. Sensitive measurement of optical nonlinearities using a single beam. *IEEE J. Quantum Electron.* **1990,** *26* (4), 760-769.
(38) Sheik-Bahae, M.; Hutchings, D. C.; Hagan, D. J.; Stryland, E. W. V. Dispersion of bound electron nonlinear refraction in solids. *IEEE J. Quantum Electron.* **1991,** *27* (6), 1296-1309.
(39) Jiang, X.; Zhang, L.; Liu, S.; Zhang, Y.; He, Z.; Li, W.; Zhang, F.; Shi, Y.; Lü, W.; Li, Y., et al. Ultrathin Metal–Organic Framework: An Emerging Broadband Nonlinear Optical Material for Ultrafast Photonics. *Advanced Optical Materials* **2018,** *6* (16), 1800561.
(40) Lu, L.; Tang, X.; Cao, R.; Wu, L.; Li, Z.; Jing, G.; Dong, B.; Lu, S.; Li, Y.; Xiang, Y., et al. Broadband Nonlinear Optical Response in Few-Layer Antimonene and Antimonene Quantum Dots: A Promising Optical Kerr Media with Enhanced Stability. *Advanced Optical Materials* **2017,** *5* (17), 1700301.
(41) Ge, Y.; Zhu, Z.; Xu, Y.; Chen, Y.; Chen, S.; Liang, Z.; Song, Y.; Zou, Y.; Zeng, H.; Xu, S., et al. Broadband Nonlinear Photoresponse of 2D TiS2 for Ultrashort Pulse Generation and All-Optical Thresholding Devices. *Advanced Optical Materials* **2018,** *6* (4), 1701166.
(42) Jiang, X.; Liu, S.; Liang, W.; Luo, S.; He, Z.; Ge, Y.; Wang, H.; Cao, R.; Zhang, F.; Wen, Q., et al. Broadband Nonlinear Photonics in Few-Layer MXene Ti3C2Tx (T = F, O, or OH) (Laser Photonics Rev. 12(2)/2018). *Laser & Photonics Reviews* **2018,** *12* (2), 1870013.
(43) Shinkawa, K.; Ogusu, K. Pulse-width dependence of optical nonlinearities in As2Se3 chalcogenide glass in the picosecond-to-nanosecond region. *Opt. Express* **2008,** *16* (22), 18230-18240.